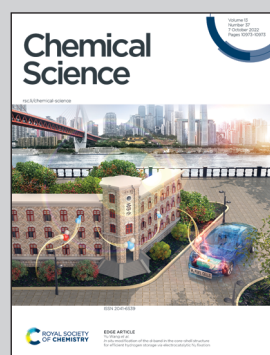


Showcasing research from the laboratories of Assoc. Prof Berggren, Department of Chemistry, University of Uppsala, Uppsala, Sweden and Dr Rodriguez-Macia, Department of Chemistry, University of Oxford, Oxford, UK.

Investigating the role of the strong field ligands in [FeFe] hydrogenase: spectroscopic and functional characterization of a semi-synthetic mono-cyanide active site

In this work, an asymmetric mono-cyanide active-site cofactor has been used to reconstitute two different [FeFe] hydrogenase scaffolds. This allowed us to investigate both the influence of the strong field ligands of the H-cluster and the impact of the host protein on the reactivity of the resulting semi-synthetic hydrogenases. Our findings show that fully reversible and fast catalysis can be achieved despite replacing a cyanide with a carbonyl ligand, but the choice of host protein dramatically influences the activity. This illustrates how, by combining different protein scaffolds and synthetic cofactors, molecular design can manipulate catalytic rate, thermodynamic driving force and inhibitor sensitivity as decoupled parameters.

## As featured in:



See Patricia Rodríguez-Maciá,  
Gustav Berggren *et al.*,  
*Chem. Sci.*, 2022, **13**, 11058.



Cite this: *Chem. Sci.*, 2022, **13**, 11058

All publication charges for this article have been paid for by the Royal Society of Chemistry

Received 22nd April 2022

Accepted 5th August 2022

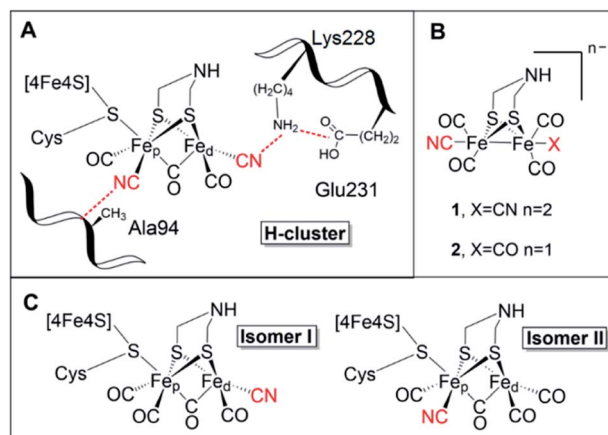
DOI: 10.1039/d2sc02271k

rsc.li/chemical-science

## Introduction

[FeFe] hydrogenases are gas-processing enzymes, catalyzing the interconversion of  $H^+$  and  $H_2$ . They have been extensively studied due to their remarkable efficiencies,<sup>1</sup> and often serve as model systems for (redox) catalysis.<sup>2–4</sup> Albeit a diverse enzyme family, all [FeFe] hydrogenases feature the so-called H-domain that harbors the active-site, which contains a hexanuclear iron complex: the “H-cluster” (Fig. 1, panel A). The H-cluster can be regarded as a canonical iron–sulfur cluster ( $[4Fe-4S]_H$ ) connected to an organometallic binuclear iron complex ( $[2Fe]_H$ ) via a bridging cysteine. Each iron ion in the  $[2Fe]_H$  subsite is further coordinated by one terminal CO and  $CN^-$  ligand while its dimeric structure is enforced by a bridging CO and an azadithiolate ligand ( $-SCH_2NHCH_2S-$ , adt).<sup>5–8</sup> Thus, the only protein derived ligand of the  $[2Fe]_H$  subsite is the cysteine that connects it to the  $[4Fe-4S]$  cluster. Still, the  $[2Fe]_H$  subsite is further anchored to the protein matrix through electrostatic

interactions involving the cyanide ligands and specific active-site pocket residues (Fig. 1, panel A). The importance of the latter binding is underscored by the observation that those residues are among the few that are strictly conserved within all known subclasses of [FeFe] hydrogenase.<sup>9–11</sup> A key structural feature of  $[2Fe]_H$  is the so-called “rotated structure” of the distal Fe ion ( $Fe_d$ ), with a bridging CO ligand and two diatomic ligands in a basal position. This geometry is considered critical



<sup>a</sup>Department of Chemistry – Ångström, Molecular Biomimetics, Uppsala University, Lägerhyddsvägen 1, 75120 Uppsala, Sweden. E-mail: Gustav.berggren@kemi.uu.se

<sup>b</sup>Department of Chemistry, Inorganic Chemistry Laboratory, University of Oxford, South Parks Road, OX1 3QR, UK. E-mail: patricia.rodriguezmacia@chem.ox.ac.uk

<sup>c</sup>Laboratoire de Chimie et Biologie des Métaux, iRTSV-LCBM/Biocat, Commissariat à l'Energie Atomique (CEA) Grenoble, 17, Rue des Martyrs, UMR 5249, 38054 Grenoble, Cedex 09, France

<sup>d</sup>Department of Chemistry – Ångström, Physical Chemistry, Uppsala University, Lägerhyddsvägen 1, 75120 Uppsala, Sweden

† Electronic supplementary information (ESI) available: Including experimental details, additional FTIR spectra and PFE data. See <https://doi.org/10.1039/d2sc02271k>

‡ These authors contributed equally.

Fig. 1 (A) Schematic representation of the active site of [FeFe] hydrogenase, the H-cluster, and selected amino acids (numbering based on CrHydA1). (B) The synthetic mimics used in this study  $[Fe_2(\mu\text{-adt})(CO)_4(CN)]^{2-}$  (1) and  $[Fe_2(\mu\text{-adt})(CO)_5(CN)]^-$  (2). (C) Possible H-cluster isomer forms following maturation of apo-hydrogenase using complex 2. Cyanide ligands are highlighted in red. Possible rotamers of isomer II are shown in Fig. S9.†



for enabling heterolytic cleavage of  $\text{H}_2$  *via* a frustrated Lewis pair (FLP) mechanism involving the open coordination site placed in an apical position of the  $\text{Fe}_d$  ion and the amine group of the adt ligand. Generating structural and functional mimics of the H-cluster and the  $[\text{2Fe}]_{\text{H}}$  subsite has been the focus of intense efforts in the organometallic community.<sup>12</sup>

The strong field ligands CO and  $\text{CN}^-$  are highly unusual in biology, but are critical for stabilizing the Fe ions in low oxidation and spin states. The  $[\text{2Fe}]_{\text{H}}$  subsite cycles between  $\text{Fe}(\text{II})$  and  $\text{Fe}(\text{I})$  during the catalytic cycle, with the so-called super reduced state representing the most reduced catalytic intermediate. The latter has been described with a  $\text{Fe}(\text{I})\text{Fe}(\text{I})$  valence in the binuclear site and a reduced  $[\text{4Fe}-\text{4S}]_{\text{H}}^+$  cluster.<sup>13</sup>

The biosynthesis and insertion of the  $[\text{2Fe}]_{\text{H}}$  subsite is dependent on a minimum of three  $[\text{FeFe}]$  hydrogenase-specific maturation enzymes.<sup>14</sup> Standard heterologous expression of these enzymes consequently yields inactive apo- $[\text{FeFe}]$  hydrogenase, containing the  $[\text{4Fe}-\text{4S}]_{\text{H}}$  cluster, but lacking the  $[\text{2Fe}]_{\text{H}}$  subsite.<sup>15</sup> However, the maturation machinery can be circumvented *via* the process of “artificial maturation”. Indeed, apo- $[\text{FeFe}]$  hydrogenase treated with the synthetic  $[\text{2Fe}]_{\text{H}}$  mimic  $[(\mu\text{-adt})\text{Fe}_2(\text{CO})_4(\text{CN})_2]^{2-}$  (**1**) (Fig. 1, panel B) yields an enzyme identical to the one found in nature, and alternative cofactors can be generated *via* suitable synthetic  $[\text{2Fe}]_{\text{H}}$  pre-cursors.<sup>7,16</sup> Artificial maturation has to-date primarily been a tool for elucidating mechanistic aspects of native  $[\text{FeFe}]$  hydrogenases,<sup>17</sup> but it also holds the promise of developing semi-synthetic hydrogenases with new properties operating both *in vitro* and *in vivo*.<sup>7,18,19</sup>

A wide range of semi-synthetic hydrogenases incorporating structurally modified  $[\text{2Fe}]_{\text{H}}$  mimics have been reported, although few have been studied in-depth.<sup>20-22</sup> In this context, the mono-cyanide version of complex **1**,  $[(\mu\text{-adt})\text{Fe}_2(\text{CO})_5(\text{CN})]^-$  (**2**) (Fig. 1, panel B), represents a particularly intriguing model to elucidate the role of the biologically unique ligand structure of the H-cluster. Other than complex **1**, and its azadiselenate analogue,<sup>7,18,21</sup> complex **2** is the only reported  $[\text{2Fe}]_{\text{H}}$  mimic capable of generating a semi-synthetic hydrogenase with significant catalytic activity for  $\text{H}_2$  conversion, as observed in earlier screening efforts.<sup>20</sup> However, as no detailed characterization of the system has been reported to-date, how complex **2** achieves its high activity upon incorporation into the HydA1 hydrogenase scaffold from *Chlamydomonas reinhardtii* (*Cr*HydA1) remains to be understood.

Apart from its activity when incorporated into *Cr*HydA1, complex **2** is also highly interesting from a molecular design perspective. It not only features a decreased negative charge relative to **1**, but the complex also displays intrinsic asymmetry. Consequently, **2** can yield two different isomers of the resulting semi-synthetic H-cluster (Fig. 1, panel C). Each of these two isomers would lack the second-coordination sphere interactions associated with either the proximal (pCN) or distal (dCN) cyanide ligand, which by extension could result in different ligand geometries of the  $[\text{2Fe}]_{\text{H}}$  subsite. Thus, semi-synthetic  $[\text{FeFe}]$  hydrogenases incorporating **2** allow us to probe both the influence of electron density as well as structural factors on the reactivity of the H-cluster.

Herein, we report the characterization of **2** incorporated into two different  $[\text{FeFe}]$  hydrogenase scaffolds, *i.e.* the monomeric HydA1 enzyme from *Chlamydomonas reinhardtii* (*Cr*) and the dimeric HydAB from *Desulfovibrio desulfuricans* (*Dd*). The active-site pocket of both enzymes is well-conserved. However, the *Dd*HydAB enzyme also contains two additional  $[\text{4Fe}-\text{4S}]$  clusters (so-called F-clusters), which serve as relays to ensure efficient electron transfer between the buried active site and the protein surface.<sup>1</sup> Our data shows that the mono-cyanide complex is able to bind the  $[\text{4Fe}-\text{4S}]_{\text{H}}$  cluster and strongly favours isomer II in both hydrogenase scaffolds (Fig. 1, panel C). Still, the H-clusters display distinct electronic structures in HydA1 and HydAB. Interestingly, the activity of the resulting semi-synthetic hydrogenase is strongly dependent on the choice of host protein.

## Results and discussion

Complex **2** was successfully introduced into the two different  $[\text{FeFe}]$  hydrogenase enzymes to yield 2-HydA1 and 2-HydAB, respectively. Similar to what is observed during maturation with complex **1**, the reaction with **2** proceeded rapidly with HydA1, while incubation for 48 h was required with HydAB. After purification, both of the resulting holo-enzymes displayed distinct FTIR spectra, with sharp H-cluster-like features (Fig. 2 and Table S1†), indicative of the complex being inserted inside the protein scaffold.<sup>7</sup> The ‘as prepared’ 2-HydAB FTIR spectrum (Fig. 2, panel A) displays a pure state represented by five narrow bands. Four distinct sharp bands in the  $1800-2000\text{ cm}^{-1}$  region ( $1835, 1903, 1923$  and  $1969\text{ cm}^{-1}$ ) corresponding to the four CO ligands, and one high-energy band at  $2057\text{ cm}^{-1}$  corresponding to the  $\text{CN}^-$  ligand. We note that the lower frequency CO band ( $1835\text{ cm}^{-1}$ ) appears at higher energy than the bridging CO ( $\mu\text{-CO}$ ) in the  $\text{H}_{\text{ox}}$  and  $\text{H}_{\text{red}}$  states of the ‘native-like’ **1**-HydAB ( $1802$  and  $1789\text{ cm}^{-1}$ , respectively), potentially reflecting a ‘semi-bridging’ CO ligand as previously proposed for the  $\text{H}_{\text{red}}\text{H}^+$  state.<sup>13,23</sup> In stark contrast to the ‘native-like’ **1**-HydAB, 2-HydAB is not sensitive to light,<sup>24</sup> and no change in the IR spectrum was observed after exposing the ‘as prepared’ sample to white-light overnight (data not shown).

The FTIR spectrum of 2-HydA1 displayed an overall spectral shape similar to that of 2-HydAB, albeit shifts of up to  $60\text{ cm}^{-1}$  are observed for low and high frequency bands. Additional broader bands were also present in the spectrum, attributable to complex **2** adventitiously binding to the surface of the enzyme (indicated at  $2044$  and  $2013\text{ cm}^{-1}$  in Fig. 2, panel B). Indeed, these broad features can be reproduced by maturing a metal-free HydA1 protein scaffold, lacking the anchoring  $[\text{4Fe}-\text{4S}]_{\text{H}}$  cluster (Fig. S1,† panel A). Moreover, the broad features exhibit light sensitivity, greatly fading upon white light illumination (Fig. S1,† panel B). Conversely, the sharp bands associated with the H-cluster appeared practically insensitive to light also in 2-HydA1. More specifically, the spectrum of light-treated 2-HydA1 is also dominated by one set of five ligand bands (Fig. 2, panel B, as prepared). The same bands were observed in the original report on 2-HydA1,<sup>20</sup> although in combination with additional signals. As compared to 2-HydAB,



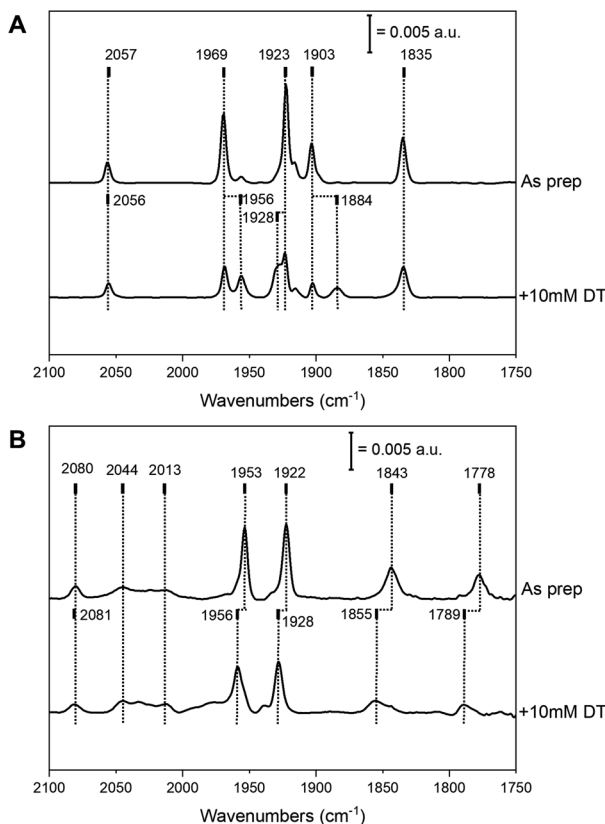


Fig. 2 FTIR spectra obtained for 2-HydAB and 2-HydA1. (A): FTIR spectra of 2-HydAB 'as prepared' (upper trace) and 10 mM NaDT reduced (bottom trace), recorded in a transmission cell ( $[2\text{-HydAB}] \approx 1 \text{ mM}$ ). (B): FTIR spectra of 2-HydA1 'as prepared' after white-light treatment (upper trace) and 10 mM NaDT reduced (bottom trace), recorded on a hydrated film by ATR-FTIR. The most prominent bands are marked by dotted lines and the corresponding frequencies are indicated on top. Spectra collected at room temperature in pH 8 buffer, with a  $2 \text{ cm}^{-1}$  spectral resolution.

the presence of a broad signal at a low energy ( $1778 \text{ cm}^{-1}$ ) is particularly noteworthy. This band is substantially lower in energy than the  $\mu\text{-CO}$  band in 'native-like' 1-HydA1. This strongly supports the presence of a  $\mu\text{-CO}$  ligand in 2-HydA1.

In both 2-HydA1 and 2-HydAB, only one distinct CN band is observable, at  $2080$  and  $2057 \text{ cm}^{-1}$  respectively, in contrast to what is observed for apo-[FeFe] hydrogenases matured with complex 1 (a summary of observed band positions and a comparison to 1-HydA1 and 1-HydAB is provided in Table S1†).<sup>17,25</sup> In combination with the distinct positions for the CO vibrations, this confirms the mono-cyanide nature of the obtained H-cluster variants in both host proteins. In addition, our data supports the notion that the H-cluster population in the 'as prepared' samples is highly homogeneous in both 2-HydA1 and 2-HydAB, suggesting that the active-site pocket strongly favors one possible isomer (Fig. 1, panel C). However, the frequency differences of the bands in the FTIR spectra (e.g. the large shift of the low frequency CO band,  $1778 \text{ cm}^{-1}$  and  $1835 \text{ cm}^{-1}$  for 2-HydA1 and 2-HydAB respectively) reveals variations in the geometry and potentially oxidation state of the  $[2\text{Fe}]_H$  subsite in the two enzymes.

Addition of the reducing agent sodium dithionite (NaDT,  $E^{0'} = -0.66 \text{ V vs. NHE}$ ) to 2-HydA1 triggered a hypsochromic (blue-)shift of several bands (Fig. 2, panel B), instead of the expected bathochromic (red-)shifts usually associated with reduction of the H-cluster. The two states observed in the presence and absence of NaDT rationalizes the FTIR spectra originally reported for 2-HydA1, as they appear to reflect a mixture of these two species.<sup>20</sup> 2-HydAB displayed more limited reactivity towards NaDT, but partial formation of a new state was discernible from new bands appearing at  $1956$ ,  $1928$  and  $1884 \text{ cm}^{-1}$  (Fig. 2, panel A). The magnitude of the shifts implies that they arise from reduction of the  $[4\text{Fe}-4\text{S}]_H$  cluster or the F-clusters, rather than the  $[2\text{Fe}]_H$  subsite.<sup>26,27</sup> Addition of the stronger reductant, Eu-DTPA ( $E^{0'} = -1.09 \text{ V vs. NHE}$ ) also did not cause complete H-cluster conversion, but resulted in a clearly discernible hypsochromic shift of the high and low frequency bands (Fig. S2†).

Electron paramagnetic resonance (EPR) spectroscopy was employed to obtain additional insight into the structure and oxidation states of the modified H-clusters. Surprisingly, EPR spectra of as-prepared 2-HydA1 (Fig. 3) show a mixture of two different rhombic signals, in contrast with the single set of peaks showing up in FTIR. We attribute this discrepancy to the cryogenic temperatures employed for the EPR measurements. Low temperatures can be expected to freeze different conformations, or rotamers, of the H-cluster that would instead average out in room temperature spectroscopy (Fig. S9†), as observed for related model complexes.<sup>28</sup> Distinct effects of applying cryogenic temperatures have also been observed for the native H-cluster.<sup>29,30</sup> More specifically, a rotation of the distal iron has previously been proposed to occur upon CO inhibition of the H-cluster,<sup>31</sup> and increased structural flexibility is in line with a more facile rotation of the non-cyanide ligated

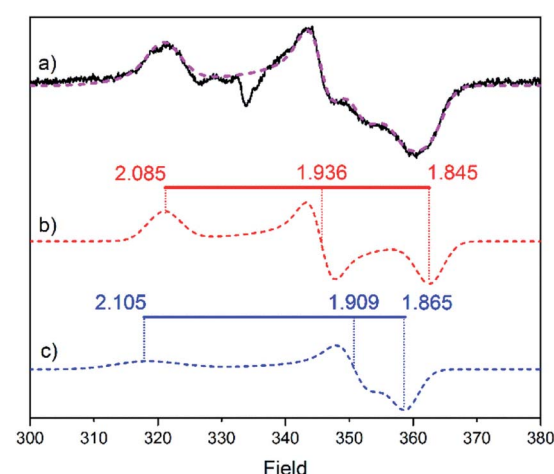


Fig. 3 EPR spectrum recorded on a 2-HydA1 ( $150 \mu\text{M}$ ) in  $100 \text{ mM}$  Tris buffer pH 8 +  $200 \text{ mM}$  KCl. (a) Experimental data (black) is overlaid with the simulated spectrum (pink dashed line) obtained fitting two rhombic signals. (b) Simulated spectrum of the first rhombic signal ( $g_{zyx} = 2.085$   $1.936$   $1.845$ ). (c) Simulated spectrum of the second rhombic signal ( $g_{zyx} = 2.105$   $1.909$   $1.865$ ). Experimental parameters: frequency:  $9.365 \text{ GHz}$ , temperature =  $10 \text{ K}$ ; microwave power =  $64 \mu\text{W}$ .

Fe ion, as it would lack the aforementioned stabilizing H-bonding interactions. Moreover, the relatively large anisotropy of the EPR signals and their fast relaxation indicate that both components of the spectrum belong to species with unpaired spin density localized on the  $[4\text{Fe}-4\text{S}]_{\text{H}}$  cluster. These results point toward the H-cluster of 2-HydA1 residing in a “super-reduced-like” state (*i.e.*  $[4\text{Fe}-4\text{S}]^{2+}-[\text{Fe}^{\text{I}}\text{Fe}^{\text{I}}]_{\text{H}}$ ) under conditions that generally yield the oxidized resting state  $\text{H}_{\text{ox}}$  (*i.e.*  $[4\text{Fe}-4\text{S}]^{2+}-[\text{Fe}^{\text{II}}\text{Fe}^{\text{I}}]_{\text{H}}$ ) in native  $[\text{FeFe}]$ -hydrogenase. Conversely, EPR spectra recorded on as-prepared samples of 2-HydAB did not reveal any discernible signal, further supporting the idea that the enzymes stabilize two different oxidation states of the modified H-cluster. We attribute the EPR silent as-prepared form of 2-HydAB to an  $\text{H}_{\text{red}}\text{H}^+$ -like oxidation state (*i.e.*  $[4\text{Fe}-4\text{S}]^{2+}-[\text{Fe}^{\text{II}}\text{Fe}^{\text{I}}]_{\text{H}}$ ). A di-ferric  $[\text{Fe}^{\text{II}}\text{Fe}^{\text{II}}]_{\text{H}}$  subsite could also explain the lack of EPR signal. However, we consider this assignment highly unlikely considering the relatively low frequencies of the carbonyl ligand vibrations. Moreover, considering their relative sigma donating properties, exchanging a CN ligand by a CO ligand will result in stabilization of lower oxidation states.

The FTIR data strongly supports the notion of selective formation of one of the two possible isomers, still the question remained open on which was being predominantly formed. To further address this issue, we prepared variants of HydA1 *via* site-directed mutagenesis, targeting amino acids in the  $[2\text{Fe}]_{\text{H}}$  second and third coordination sphere of the cyanides of the native co-factor (Fig. 1, panel A). In the case of dCN, its environment is closely connected to the maturation channel by which the  $[2\text{Fe}]_{\text{H}}$  precursor is suggested to enter the active-site.<sup>15,32</sup> Thus, we decided to prepare the third-coordination sphere E231D variant targeting a glutamate residue involved in a salt-bridge with Lysine228, which in turn is thought to be important to fix the distal CN position. Interestingly, despite repeated efforts, maturation of this mutant with complex 2 could not be achieved. This agrees with previous reports of Lysine228 as the last amino acid in the positively charged maturation channel. Mutations interfering with its positioning unavoidably generate variants defective in cofactor incorporation.<sup>32,33</sup> Thus, the A94S variant was also prepared, targeting an alanine residue known to be directly interacting with pCN. The introduction of a polar side chain in this position influences the cyanide stretching mode,<sup>33</sup> and causes a distinct red-shift of the only identifiable CN band of 2-HydA1<sup>A94S</sup> by  $20\text{ cm}^{-1}$  (Fig. S3†). The effect of the A94S mutation can also be observed as a  $3-5\text{ cm}^{-1}$  blue-shift on two CO bands. The comparison is complicated by the appearance of two extra bands in the 2-HydA1<sup>A94S</sup> FTIR spectrum, at  $1959$  and  $1936\text{ cm}^{-1}$ . As the preparation protocol is identical to that of the wild-type enzyme, they can only be attributed to the introduction of this point-mutation. It is possible that the introduction of a polar residue, which can also act as hydrogen bond donor, could trigger the formation of additional conformations for the mono-CN H-cluster in 2-HydA1<sup>A94S</sup>. Alternatively, the effect of the mutation could be that of slowing down ligand rotation resulting in an observation analogous to the double signal seen with EPR. Regardless, the distinct shifts observed for the CO bands and in particular the CN band provide compelling

evidence for the occurrence of isomer II (Fig. 1, panel C) as the predominant conformation for 2-HydA1. Indeed, the observed shift are strikingly similar to earlier observations with the HydA1<sup>A94S</sup> variant also for the native cofactor (1-HydA1<sup>A94S</sup>).<sup>33</sup> The formation of isomer II is also indirectly supported by the reactivity observed towards the well-known inhibitors CO and  $\text{O}_2$ . Exposing 2-HydA1 to air resulted in appearance of a small population of a species reminiscent of the  $\text{H}_{\text{ox}}$ -air state observed in TamHydS (Fig. S4†).<sup>34</sup> As this state is thought to feature a partially decomposed  $[2\text{Fe}]_{\text{H}}$  subsite with a single Fe ion coordinated by the bridging cysteine, the presence of a band attributable to Fe coordinated CN in this spectrum is consistent with the loss of an all-carbonyl distal Fe ion of isomer II.

In the case of 2-HydAB, the enzyme also exhibits unusual reactivity towards  $\text{O}_2$ , displaying substantially lower  $\text{O}_2$  sensitivity compared with the native-like 1-HydAB. The IR signature of 2-HydAB was significantly more long-lived than that of 1-HydAB after exposing the two enzymes to air, retaining 45% of the IR signal intensity after 30 min of air exposure for 2-HydAB compared with only 16% after 5 min of exposing 1-HydAB to air (Fig. S5†).

In contrast to the eventual degradation under air, both 2-HydAB and 2-HydA1 appeared completely unreactive towards CO. This is remarkable, as CO is a well-known competitive inhibitor of hydrogenases.<sup>35</sup> Especially 1-HydAB has a very high affinity toward CO, and is often isolated in a CO inhibited state ( $\text{H}_{\text{ox}}-\text{CO}$ ).<sup>35,36</sup> However, incubation of as-prepared 2-HydAB under a neat  $\text{N}_2$  atmosphere for up to 48 h to promote CO release did not result in any significant difference in the FTIR spectrum, strongly arguing against the as-prepared spectrum representing a CO inhibited form of the enzyme. Likewise, exposing as prepared samples of 2-HydA1 and 2-HydAB to 1 atm CO for up to one hour, did not alter the state of the sample, and no extra IR bands could be detected in the IR spectrum (data not shown). Finally, 2-HydAB and 2-HydA1 were treated with one equivalent of KCN to explore the possibility of generating the native di-cyanide cofactor *via* post-synthetic exchange of a CO ligand. However, after 60 minutes of incubation at pH 8 and room temperature, the FTIR spectra revealed no formation of new species (*e.g.* no extra CN or CO bands) either for 2-HydAB or 2-HydA1 (data not shown).

Both the band positions of the FTIR spectrum and the characteristics of the EPR signals reveal that the H-cluster of 2-HydA1 and 2-HydAB are clearly distinct from the native H-cluster. Moreover, the decreased anionic charge of complex 2 is expected to result in more positive reduction potentials compared to complex 1.<sup>37</sup> We investigated how these changes in redox and structural properties would impact the catalytic behavior of the semi-synthetic mono-cyanide  $[\text{FeFe}]$  hydrogenases, using a combination of protein film electrochemistry (PFE) and solution activity assays.

As reported by Siebel and coworkers, 2-HydA1 maintains a significant amount of residual  $\text{H}_2$  evolution activity. In our hands 2-HydA1 show  $\text{H}_2$  evolution activity values of  $223 \pm 25\text{ }\mu\text{mol H}_2\text{ mg}_{\text{protein}}^{-1}\text{ min}^{-1}$ , whereas samples of 1-HydA1 display a  $\text{H}_2$  evolution activity of  $370 \pm 64\text{ }\mu\text{mol H}_2\text{ mg}_{\text{protein}}^{-1}\text{ min}^{-1}$ . In contrast, 2-HydAB only showed a 1% residual activity for  $\text{H}_2$



production ( $84 \pm 13 \mu\text{mol mg}_{\text{protein}}^{-1} \text{ min}^{-1}$ ) and 0.02% residual activity for  $\text{H}_2$  oxidation ( $15.23 \pm 0.57 \mu\text{mol mg}_{\text{protein}}^{-1} \text{ min}^{-1}$ ).

Similarly, cyclic voltammograms (CVs) recorded with PFE following adsorption of 2-HydAB onto a rotating-disk pyrolytic graphite edge (PGE) electrode, showed only small residual electrocatalytic currents attributable to  $\text{H}^+$  reduction and  $\text{H}_2$  oxidation (Fig. S6†). Care should be taken when attributing significance to absolute currents in PFE, as it reflects both intrinsic enzyme activity as well as enzyme coverage on the electrode surface. Still, the CV for 2-HydAB is in line with the data obtained from solution activity assays where only residual activity for both  $\text{H}_2$  production and  $\text{H}_2$  oxidation was detected. The inactive nature of 2-HydAB is remarkable, as the native-like 1-HydAB is one of the most active semi-synthetic [FeFe] hydrogenases studied so far, operating reversibly over a wide pH range.<sup>26,35,38</sup> Thus, we conclude that in the case of HydAB, the mono-cyanide semi-synthetic enzyme dramatically lowers its activity for  $\text{H}_2$  conversion.

Conversely, CVs of 2-HydA1 absorbed on a PGE electrode show electrocatalytic current in both directions, displaying the typical behavior of a reversible catalyst, with no overpotential requirement either in the oxidative or in the reductive direction (Fig. 4 and S7†). The Michaelis constant ( $K_m$ ) for  $\text{H}_2$  was determined to be above 1 atm through chronoamperometric studies under continuously varying  $\text{H}_2$  concentration (Fig. S8†), as compared to  $0.64 \pm 0.05$  atm reported for 1-HydA1.<sup>39</sup> Additionally, the intrinsic catalytic bias of 2-HydA1 was estimated from the ratio between oxidative and reductive currents at 100 mV over-potential. The observed ( $i_{\text{ox}}/i_{\text{red}}$ ) ratio of  $\approx 1.6$  indicates a bias towards  $\text{H}_2$  oxidation, comparable to what is observed for 1-HydA1 ( $i_{\text{ox}}/i_{\text{red}} \approx 1.5$ ).

## Conclusions

In summary, the unsymmetrical H-cluster generated *via* artificial maturation with the monocyanide complex 2 has been functionally and spectroscopically characterized in-detail. The study employed two different hydrogenase scaffolds, also providing insight into how the protein scaffold tunes the active-site properties. Apart from the complex  $[(\mu\text{-pdt})\text{Fe}_2(\text{CO})_4(-\text{CN})_2]^{2-}$  (3, pdt =  $-\text{SCH}_2\text{CH}_2\text{CH}_2\text{S}-$ ), which is analogous to complex 1 but the adt amine is replaced by a methylene group, this is the first time that an H-cluster variant has been prepared and characterized in *Dd*HydAB. In a hydrogenase context, this study sheds new light on the role of both the primary and secondary coordination sphere in structure and reactivity of the H-cluster. The reactivity of 2-HydA1 implies that the presence of a symmetric di-cyanide cofactor in native [FeFe] hydrogenase is not a strict requirement from an electron density perspective. The decreased electron density of the mono-cyanide variant could also at least partially rationalize the lower affinity for binding additional CO ligands, as it lowers the capacity of the  $[\text{2Fe}]_{\text{H}}$  subsite for  $\pi$  back-bonding.

In light of these observations, the symmetric di-atomic ligand pattern of the native  $[\text{2Fe}]_{\text{H}}$  subsite is likely an adaptation to the biosynthesis of the  $[\text{2Fe}]_{\text{H}}$  subsite, proceeding *via* dimerization of two  $\text{Fe}(\text{CO})_2\text{CN}$  synthons.<sup>40,41</sup> In native [FeFe] hydrogenase a high tolerance towards CO can be achieved *via* changes to the protein scaffold but appears to be connected to a significant decrease in catalytic efficiencies, as exemplified by the putative sensory hydrogenases from *Thermoanaerobacter mathranii*<sup>34,42</sup> and *Thermotoga maritima*.<sup>43</sup> Thus, a mono-cyanide cofactor could provide an evolutionary advantage, as it can combine high activity and CO tolerance. However, it would come with a significant cost, as it would require at least one additional enzyme in the maturation machinery complementing HydG to produce a suitable monomeric Fe-ion precursor.

With regards to the second coordination sphere, K228 (*Cr*HydA1 numbering) is an extremely well conserved residue, and its interaction with the dCN ligand is thought to play a key role in stabilizing the rotated structure of the distal iron, and preventing the formation of dead-end intermediates.<sup>44</sup> However, it has been challenging to probe directly, as H-cluster assembly is prevented in K228 variants.<sup>45</sup> Despite the inactivity of 2-HydAB, the results for 2-HydA1 shows that the distal CN ligand (dCN), and by extension its H-bonding interactions, does not represent a critical structural feature for catalysis. Still, we note that K228 might be needed for decreasing the electron donation of dCN in the native di-cyanide cofactor.

Additionally, the K228-dCN interaction evidently contributes to the stabilization of the specific rotamer constituting the rotated structure (Fig. 1 and S9†), which holds the open coordination site in an apical position. This notion is supported by the observation of two separate H-cluster species in low temperature EPR measurements of 2-HydA1. In parallel, the significant loss of activity in 2-HydAB can be attributed to the stabilization of an inactive rotamer in the absence of the dCN-K228 interaction (Fig. S9†, rotamer I or II). This is in line with

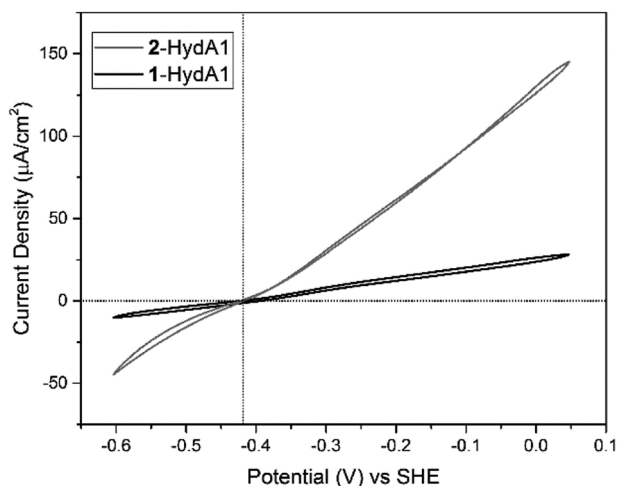


Fig. 4 Cyclic voltammograms of 2-HydA1 (black trace) and 1-HydA1 (grey trace) films absorbed on a rotating-disk PGE electrode, measured in pH 7 buffer mix in the absence of halides under 1 atm  $\text{H}_2$  gas, scan rate: 10 mV s<sup>-1</sup>, temperature: 30 °C and rotation rate: 3000 rpm. The vertical dotted-line indicates the thermodynamic potential for the  $2\text{H}^+/\text{H}_2$  couple at pH 7 ( $E^0 = -0.413 \text{ V}$ , vs. SHE), while the horizontal dotted-line represent the zero current.



the exceptional stability of the CO-inhibited state  $H_{ox}$ -CO in native *Dd*HydAB.<sup>35</sup> The high affinity of *Dd*HydAB towards CO is not well understood yet. However, it implies a strong tendency to stabilize a CO ligand in the apical position of the distal Fe ion. We hypothesize that in 2-HydAB, lacking the H-bonding interactions of the dCN ligand enforcing the “rotated structure”, one of the CO ligands of the distal Fe ion is likely to be stabilized in the apical position. This would result in a rotamer where the vacant site is not at the apical position, thus losing the critical FLP interaction with the adt-nitrogen, rationalizing the catalytically inactive nature 2-HydAB (Fig. S9,† rotamers I or II). Such a structural arrangement is likely to be an additional factor contributing to the enhanced  $O_2$  and CO tolerance of 2-HydAB, as it would decrease inhibitor accessibility to the  $[2Fe]_H$  subsite. In short, formation of the key rotated structure must be triggered primarily by other interactions in the active site pocket or protein surrounding, and then subsequently stabilized by K228.

From a molecular design perspective, the 2-HydA1 system allowed us to probe the effect of the H-cluster on the overall catalytic performance in a direct way: exchange of a CN for CO causes a slight decrease in rate for  $H_2$  production and an increase in  $K_m$ , but comes with significant improvements in inhibition tolerance. Furthermore, it does not introduce an over-potential for catalysis in any direction. In a broader context, the reactivity observed for 2-HydA1 provides an example of how rate and over-potential for catalysis are decoupled parameters in (redox) catalysis.<sup>2,3</sup> Finally, this study shows that it is possible to rely on the protein scaffold to introduce asymmetric mimics in the hydrogenase active site in a selective fashion, paving the way for highly elaborate catalyst design. Moreover, the observed differences in catalytic activity of 2-HydAB and 2-HydA1 highlights the importance of exploring different hydrogenase scaffolds when constructing semi-synthetic hydrogenases.

## Author contributions

Conceptualization: M. L., G. B. and P. R.-M.; methodology: M. L., J. G., P. R.-M.; investigation: M. L., J. G., A. Z., M. S. Z. D.; writing – original draft: M. L., G. B. and P. R.-M.; writing – review & editing: all authors; supervision: G. B. and P. R.-M.; funding acquisition: G. B. and P. R.-M.

## Conflicts of interest

There are no conflicts to declare.

## Acknowledgements

The European Research Council (ERC, to GB, Contract No. 714102) as well as the European Union's Horizon 2020 research and innovation program (Marie Skłodowska Curie Grant No. 897555 to MS) are gratefully acknowledged for funding. PR-M thanks the University of Oxford for a Glasstone Research Fellowship and Linacre College Oxford for a Junior Research Fellowship. The University of Oxford Santander/Oxford Travel

Awards is gratefully acknowledged for supporting JG's research stay at the University of Uppsala. The authors would also like to express their gratitude to Dr James Birrell for critical reading of the manuscript.

## Notes and references

- W. Lubitz, H. Ogata, O. Rudiger and E. Reijerse, *Chem. Rev.*, 2014, **114**, 4081–4148.
- V. Fourmond, N. Plumeré and C. Léger, *Nat. Rev. Chem.*, 2021, **5**, 348–360.
- V. Fourmond, E. S. Wiedner, W. J. Shaw and C. Léger, *J. Am. Chem. Soc.*, 2019, **141**, 11269–11285.
- D. W. Mulder, J. W. Peters and S. Raugei, *Chem. Commun.*, 2021, **57**, 713–720.
- J. W. Peters, W. N. Lanzilotta, B. J. Lemon and L. C. Seefeldt, *Science*, 1998, **282**, 1853–1858.
- Y. Nicolet, C. Piras, P. Legrand, C. E. Hatchikian and J. C. Fontecilla-Camps, *Structure*, 1999, **7**, 13–23.
- G. Berggren, A. Adamska, C. Lambertz, T. R. Simmons, J. Esselborn, M. Atta, S. Gambarelli, J. M. Mouesca, E. Reijerse, W. Lubitz, T. Happe, V. Artero and M. Fontecave, *Nature*, 2013, **499**, 66–69.
- A. Silakov, E. J. Reijerse, S. P. J. Albracht, E. C. Hatchikian and W. Lubitz, *J. Am. Chem. Soc.*, 2007, **129**, 11447–11458.
- L. S. Mészáros, H. Land, H. J. Redman and G. Berggren, *Curr. Opin. Green Sustainable Chem.*, 2021, **32**, 100521.
- P. Knörzer, A. Silakov, C. E. Foster, F. A. Armstrong, W. Lubitz and T. Happe, *J. Biol. Chem.*, 2012, **287**, 1489–1499.
- M. Winkler, J. Esselborn and T. Happe, *Biochim. Biophys. Acta, Bioenerg.*, 2013, **1827**, 974–985.
- J. T. Kleinhaus, F. Wittkamp, S. Yadav, D. Siegmund and U.-P. Apfel, *Chem. Soc. Rev.*, 2021, **50**, 1668–1784.
- J. A. Birrell, P. Rodríguez-Maciá, E. J. Reijerse, M. A. Martini and W. Lubitz, *Coord. Chem. Rev.*, 2021, **449**, 214191.
- R. D. Britt, G. Rao and L. Tao, *Chem. Sci.*, 2020, **11**, 10313–10323.
- D. W. Mulder, E. S. Boyd, R. Sarma, R. K. Lange, J. A. Endrizzi, J. B. Broderick and J. W. Peters, *Nature*, 2010, **465**, 248–251.
- J. Esselborn, C. Lambertz, A. Adamska-Venkatesh, T. Simmons, G. Berggren, J. Noth, J. Siebel, A. Hemschemeier, V. Artero, E. Reijerse, M. Fontecave, W. Lubitz and T. Happe, *Nat. Chem. Biol.*, 2013, **9**, 607–609.
- H. Land, M. Senger, G. Berggren and S. T. Stripp, *ACS Catal.*, 2020, **10**, 7069–7086.
- N. Khanna, C. Esmieu, L. S. Meszaros, P. Lindblad and G. Berggren, *Energy Environ. Sci.*, 2017, **10**, 1563–1567.
- L. S. Meszaros, B. Nemeth, C. Esmieu, P. Ceccaldi and G. Berggren, *Angew. Chem., Int. Ed.*, 2018, **57**, 2596–2599.
- J. F. Siebel, A. Adamska-Venkatesh, K. Weber, S. Rumpel, E. Reijerse and W. Lubitz, *Biochemistry*, 2015, **54**, 1474–1483.
- L. Kertess, F. Wittkamp, C. Sommer, J. Esselborn, O. Rudiger, E. J. Reijerse, E. Hofmann, W. Lubitz, M. Winkler, T. Happe and U. P. Apfel, *Dalton Trans.*, 2017, **46**, 16947–16958.



22 C. Sommer, C. P. Richers, W. Lubitz, T. B. Rauchfuss and E. J. Reijerse, *Angew. Chem., Int. Ed.*, 2018, **57**, 5429–5432.

23 Y. Nicolet, A. L. de Lacey, X. Vernedé, V. M. Fernandez, E. C. Hatchikian and J. C. Fontecilla-Camps, *J. Am. Chem. Soc.*, 2001, **123**, 1596–1601.

24 M. Sensi, C. Baffert, V. Fourmond, L. de Gioia, L. Bertini and C. Léger, *Sustainable Energy Fuels*, 2021, **5**, 4248–4260.

25 A. Silakov, C. Kamp, E. Reijerse, T. Happe and W. Lubitz, *Biochemistry*, 2009, **48**, 7780–7786.

26 P. Rodríguez-Maciá, K. Pawlak, O. Rüdiger, E. J. Reijerse, W. Lubitz and J. A. Birrell, *J. Am. Chem. Soc.*, 2017, **139**, 15122–15134.

27 C. Sommer, A. Adamska-Venkatesh, K. Pawlak, J. A. Birrell, O. Rüdiger, E. J. Reijerse and W. Lubitz, *J. Am. Chem. Soc.*, 2017, **139**, 1440–1443.

28 W. Wang, M. J. Nilges, T. B. Rauchfuss and M. Stein, *J. Am. Chem. Soc.*, 2013, **135**, 3633–3639.

29 C. Lorent, S. Katz, J. Duan, C. J. Kulka, G. Caserta, C. Teutloff, S. Yadav, U.-P. Apfel, M. Winkler, T. Happe, M. Horch and I. Zebger, *J. Am. Chem. Soc.*, 2020, **142**, 5493–5497.

30 S. T. Stripp, S. Mebs and M. Haumann, *Inorg. Chem.*, 2020, **59**, 16474–16488.

31 M. Senger, S. Mebs, J. Duan, F. Wittkamp, U.-P. Apfel, J. Heberle, M. Haumann and S. T. Stripp, *Proc. Natl. Acad. Sci. U. S. A.*, 2016, **113**, 8454–8459.

32 O. Lampret, J. Esselborn, R. Haas, A. Rutz, R. L. Booth, L. Kertess, F. Wittkamp, C. F. Megarity, F. A. Armstrong, M. Winkler and T. Happe, *Proc. Natl. Acad. Sci. U. S. A.*, 2019, **116**, 15802–15810.

33 O. Lampret, A. Adamska-Venkatesh, H. Konegger, F. Wittkamp, U.-P. Apfel, E. J. Reijerse, W. Lubitz, O. Rüdiger, T. Happe and M. Winkler, *J. Am. Chem. Soc.*, 2017, **139**, 18222–18230.

34 H. Land, A. Sekretareva, P. Huang, H. J. Redman, B. Németh, N. Polidori, L. S. Mészáros, M. Senger, S. T. Stripp and G. Berggren, *Chem. Sci.*, 2020, **11**, 12789–12801.

35 G. Goldet, C. Brandmayr, S. T. Stripp, T. Happe, C. Cavazza, J. C. Fontecilla-Camps and F. A. Armstrong, *J. Am. Chem. Soc.*, 2009, **131**, 14979–14989.

36 J. A. Birrell, K. Wrede, K. Pawlak, P. Rodriguez-Maciá, O. Rüdiger, E. J. Reijerse and W. Lubitz, *Isr. J. Chem.*, 2016, **56**, 852–863.

37 C. Esmieu and G. Berggren, *Dalton Trans.*, 2016, **45**, 19242–19248.

38 B. R. Glick, W. G. Martin and S. M. Martin, *Can. J. Microbiol.*, 1980, **26**, 1214–1223.

39 V. Fourmond, C. Baffert, K. Sybirna, S. Dementin, A. Abou-Hamdan, I. Meynil-Salles, P. Soucaille, H. Bottin and C. Léger, *Chem. Commun.*, 2013, **49**, 6840–6842.

40 Y. Zhang, L. Tao, T. J. Woods, R. D. Britt and T. B. Rauchfuss, *J. Am. Chem. Soc.*, 2022, **144**, 1534–1538.

41 J. M. Kuchenreuther, W. K. Myers, D. L. M. Suess, T. A. Stich, V. Pelmenschikov, S. A. Shiigi, S. P. Cramer, J. R. Swartz, R. D. Britt and S. J. George, *Science*, 2014, **343**, 424–427.

42 A. Fasano, H. Land, V. Fourmond, G. Berggren and C. Léger, *J. Am. Chem. Soc.*, 2021, **143**, 20320–20325.

43 N. Chongdar, J. A. Birrell, K. Pawlak, C. Sommer, E. J. Reijerse, O. Rüdiger, W. Lubitz and H. Ogata, *J. Am. Chem. Soc.*, 2018, **140**, 1057–1068.

44 A. R. Finkelmann, M. T. Stiebrtz and M. Reiher, *Chem. Sci.*, 2014, **5**, 215–221.

45 P. Knörzer, A. Silakov, C. E. Foster, F. A. Armstrong, W. Lubitz and T. Happe, *J. Biol. Chem.*, 2012, **287**, 1489–1499.

